Advances in Nano Research, *Vol. 12, No. 1 (2022) 25-35*
https://doi.org/10.12989/anr.2022.12.1.025

Electron transport in core-shell type fullerene nanojunction

Daulet Sergeyev*[1,2] and Ainur Duisenova[1]

[1]*Department of Physics, K. Zhubanov Aktobe Regional State University, 34A Moldagulova avenue, 030000 Aktobe, Kazakhstan*
[2]*Department of Radio Electronics, T. Begeldinov Aktobe Aviation Institute, 39 Moldagulova avenue, 030012 Aktobe, Kazakhstan*

(*Received August 3, 2021, Revised August 31, 2021, Accepted September 2, 2021*)

Abstract. Within the framework of the density functional theory combined with the method of non-equilibrium Green's functions (DFT + NEGF), the features of electron transport in fullerene nanojunctions, which are «core-shell» nanoobjects made of a combination of fullerenes of different diameters C_{20}, C_{80}, C_{180}, placed between gold electrodes (in a nanogap), are studied. Their transmission spectra, the density of state, current-voltage characteristics and differential conductivity are determined. It was shown that in the energy range of -0.45–0.45 eV in the transmission spectrum of the "Au–C_{180}–Au" nanojunction appears a HOMO–LUMO gap with a width of 0.9 eV; when small-sized fullerenes C_{20}, C_{80} are intercalation into the cavity C_{180} the gap disappears, and a series of resonant structures are observed on their spectra. It has been established that distinct Coulomb steps appear on the current-voltage characteristics of the "Au–C_{180}–Au" nanojunction, but on the current-voltage characteristics "Au–C_{80}@C_{180}–Au", "Au–(C_{20}@C_{80})@C_{180}–Au" these step structures are blurred due to a decrease in Coulomb energy. An increase in the number of Coulomb features on the dI/dV spectra of core-shell fullerene nanojunctions was revealed in comparison with nanojunctions based on fullerene C_{60}, which makes it possible to create high-speed single-electron devices on their basis. Models of single–electron transistors (SET) based on fullerene nanojunctions "Au–C_{180}–Au", "Au–C_{80}@C_{180}–Au" and "Au–(C_{20}@C_{80})@C_{180}-Au" are considered. Their charge stability diagrams are analyzed and it is shown that SET based on C_{80}@C_{180}-, (C_{20}@C_{80})@C_{180}- nanojunctions is output from the Coulomb blockade mode with the lowest drain-to-source voltage.
Keywords: Coulomb blockade; current-voltage characteristic; electron transport; fullerene; nanojunction, single–electron transistor

1. Introduction

Recently, the potential of traditional silicium-based semiconductor circuitries has been exhausted, there are many problems are unsolvable without the use of fundamentally new physical and technological ideas. One of these problems of electronics is increasing the speed of electronic systems while reducing their size and energy consumption (Cuevas and Scheer 2017, Xiang *et al.* 2020). The solution to this problem and the further development of electronics largely depend on the possibility of the emergence of new materials of electron technology. The search and synthesis of new materials with unusual properties used to create new small-sized electronic devices, and the modernization of the properties of existing materials by improving the technology of their manufacture and processing will mainly determine the progress of promising electronics. To solve the problems of miniaturization of electronic components with an increase in the degree of integration of integrated circuits, new types of electronic devices are being developed using nanomaterials with controlled electrophysical properties свойствами (Chuan *et al*. 2021, Sergeyev 2021, Montanaro *et al*. 2021).

With the discovery of graphene (Novoselov *et al.* 2004, Castro Neto *et al.* 2009) and other two-dimensional atomic crystals (Dragoman *et al*. 2019 Huang *et al.* 2020, Kiraly *et al.* 2020, Sahoo and Wei 2019) it was proposed and implemented that exotic materials of electronic technology, consisting of isolated atomic planes can be assembled in the construction of heterostructures made by layers of pre-selected sequence – van-der-Waals heterostructures. This means that if we consider two-dimensional crystals as similar to Lego blocks, it becomes possible to create a huge variety of layered structures with specified properties (Geim and Grigorieva 2013).

In terms of miniaturization of electronic components, one of the widely used materials are carbon nanomaterials – carbon nanotubes (CNT), fullerenes, graphenes and related structures (Morozov *et al.* 2008, Iijima 1991, Kroto 1985, Geim 2009, Dragoman 2017, Murali 2012, Marani *et al.* 2017). They have such unique properties as ultra-small dimensions, good electrical conductivity, high emission characteristics, high chemical stability, and the ability to attach a variety of chemical radicals to themselves (Eletskii 1997), which allow them to create new types of promising electronics elements on their basis (Kumar 2018, Kharlamova 2013, Sergeyev 2018). Note that in addition to CNT, octagraphene nanotubes also have interesting electric transport characteristics that allow them to be used in the future to create electronic devices (Sergeyev 2020a).

For the subsequent miniaturization of electronic devices, two-dimensional (2D) magnetic materials with strong magnetization at room temperature (~ 300 K) are known to be a promising material. Spin valves (Davis *et al.* 2021, Wang *et al.* 2021), spin field-effect transistors (Gyanchandani *et al*. 2021, Zhu *et al*. 2021) and magnetic

*Corresponding author, Professor,
E-mail: serdau@mail.ru

ISSN: 2287-237X (Print), 2287-2388 (Online)

tunnel junctions with spin filtration (Daqiq 2021, Yang *et al.* 2021), which are the basic elements of spintronics (Hirohata *et al.* 2020). are created on the basis of such materials.

It should be noted that one of the promising directions in terms of miniaturization and improving performance is the use of superconducting materials in integrated circuits. Based on the phenomenon of superconductivity, active elements of ultra-sensitive receiving and transmitting devices – detectors, mixers, generators, parametric amplifiers, frequency converters, etc. have already been implemented (Miao *et al.* 2021, Bal *et al.* 2021, Kalashnikov *et al.* 2018). There have been created switches and current limiters (Martini *et al.* 2006, Dalessandro *et al.* 2007), various magnetic field sensory elements and detectors, including for magnetocardiography and magnetoencephalography (Wang *et al.* 2020, Faley *et al.* 2012), voltage reference (standard volt with an accuracy of about 10^{-10}) (Burroughs *et al.* 1999), and also the core of a quantum computer – qubits (quantum bits) (Cattaneo *et al.* 2021, Lee *et al.* 2019, Macha *et al.* 2014). Josephson logic elements, characterized by high speed (low switching time) and low energy consumption, are a worthy alternative for creating integrated circuits of digital electronics (Likharev 2012, Tolpygo 2016). Josephson elements are also successfully used to create and implement ultra-sensitive receiving devices of the millimeter and sub-millimeter wavelength range. The high nonlinearity of the electrical characteristics of Josephson junctions made it possible to create receiving devices whose maximum sensitivity is limited by the quantum limit (Kornev 2017, Sergeyev 2012, 2013).

The creation of nanocircuits in which the role of functional elements is performed by individual molecules is also promising. This is one of the alternative approaches to the development of electronics – single electronics, theoretically predicted by D. V. Averin and K. K. Likharev, based on the effect of correlated tunneling of single electrons (Averin and Likharev 1986, Likharev 1999). The essence of this effect is the Coulomb blockade of electron transport and the ordered movement of elementary charges arising due to their interaction through an electric field. The construction of a SET is a three-electrode tunneling device consisting of a conducting islet molecule with a small intrinsic capacity, connected to the source and drain electrodes by tunnel junctions with a small capacity and conductivity.

The effect of correlated tunneling of single electrons has already been observed in various materials, for example, in metals, in semiconductors, in superconductors, in carbon nanostructures, molecular structures. Graphene-based transistors are considered to be promising SET (Khademhosseini *et al.* 2021, Fried *et al.* 2020) and organic molecules (Gaurav *et al.* 2019, Anu *et al.* 2018). Currently, various single-electron molecular devices have been experimentally implemented: a SET, a memory cell, and logic elements. Further development of the technology of single-electron molecular devices will allow creating memory cells with a long storage time, high data recording density and low power dissipation, as well as highly sensitive chemical and biochemical sensors.

In single-electron devices, the current flow significantly depends on the electronic structure of the molecule, since they have discrete electronic levels that can be open or closed for electron transfer in the system. This means that for the SET design, it is necessary to select molecules with unique functional properties, including structurally resistant to charge changes. One of such materials is fullerene-like materials. They have a number of remarkable characteristics for creating a SET, including chemical resistance, high strength, rigidity and good electrical conductivity. The remarkable thing is that depending on the fine features of molecular symmetry, fullerene-like materials can be dielectrics, semiconductors, have metallic and superconducting properties. These properties, combined with the nanoscale geometry, make them unique materials for their application in creating a SET. For example, the influence of electronic vibrational modes on the process of correlated electron tunneling in SET based on two covalently connected C_{70} fullerene molecules was studied in the work (Pasupathy *et al.* 2005, Champagne *et al.* 2005), a combined method was used to study the electric transport characteristics of SET, considering the combination of electrostatic control of a Coulomb Island made of C_{60} fullerene with a mechanically controlled nanojunction.

It is known that the transport of quasiparticles through individual molecules is strongly modified by the charge of one electron and the quantization of energy levels. These effects, which determine the transfer of electrons through nanosized molecules, are used to create a SET. As such SET molecules, individual C_{60} molecules are successfully used in combination with gold electrodes (Ward *et al.* 2008, Nakajima *et al.* 2015). Such SETs with a single C_{60} molecule represent a quantum "mechanical" system, due to the quantized oscillation of the C_{60} behaves like a high frequency nanomechanical generator (Park *et al.* 2000). Over time, it became clear that several factors significantly affect the electric transport properties of nanoscale devices, for example, changes in the molecular conformation, settings between the Coulomb blockade of weak coupling and the Kondo modes of strong coupling and the material of the electrode of the nanodevice. Usually, gold (Au) or other noble metals with good electrical conductivity are used as the electrode material in nanodevices, since they exhibit reduced variability of transport characteristics due to their inert nature. It should be noted that in recent years, fullerene-graphene layered nanostructures consisting of a combination of fullerenes (C_{60}) and graphene layers have been actively studied (Devi 2019, Ceron *et al.* 2019, Artyukh and Chernozatonskii 2020). Such nanomaterials are promising for solving several applied problems, such as the creation of high - efficient solar cells and an electric energy storage device (supercapacitors) (Cardenas-Jiron *et al.* 2019, Chen *et al.* 2016, Kang *et al.* 2019). A fragment of such fullerene-graphene layered systems is "graphene – fullerene – graphene" nanojunctions, where graphene is used as an electrode material. The adsorption and thermoelectric properties of such hybrid nanocontacts are studied in the works (Koh *et al.* 2015, Gehring *et al.* 2017).

Currently, the Non-Equilibrium Green's Functions

(NEGF) method is widely used to describe the transport characteristics of a molecular transistor. In the works (Sergeyev *et al*. 2021, Nasri *et al*. 2018), the transport properties of a molecular transistor on fullerenes were calculated using the NEGF method and the effects of electrode materials (gold, platinum, graphene) were shown on the transport properties of such a transistor.

It is known that one of the unique properties of fullerene structures is to enclose one or more atoms inside its carbon frame. Such structures are commonly called endohedral fullerenes (Akasaka and Nagase 2002). The electronic properties of endohedral fullerenes significantly depend on the properties of the encapsulated atom, which makes it possible to control them by selecting the encapsulated atom desired by the property. In a previous work (Sergeyev 2020b), we demonstrated the effect of encapsulated alkali metals Li, Na, K on the electric transport characteristics of a SET based on Me@C_{60} (Me = Li, Na, K).

Recently, molecular clusters made of fullerenes have attracted particular interest for the creation of SET (Hosseini *et al.* 2018). It is also known that layered (quasi) two-dimensional nanostructures also have good properties for creating single-electronics elements (Chuan *et al.* 2021, Mouafo *et al.* 2020, Sergeyev and Duisenova 2021). It is reasonable to think about what properties fullerene transistor structures have, where small-radius fullerenes are placed inside a larger-radius fullerene forming a «core-shell» type nanojunction. Here, a small – radius fullerene acts as the core, and a large-radius fullerene acts as the shell. The geometric shape of such molecular structures resembles the famous Russian nesting doll – matryoshka, which is a wooden doll, inside which there are similar smaller dolls.

In the present work, the electric transport characteristics of "Au–C_{180}–Au", "Au–C_{80}@C_{180}–Au" and "Au–(C_{20}@C_{80})@C_{180}–Au" nanojunctions are modeled and analyzed within the framework of the density functional theory (DFT) in combination with the method of nonequilibrium Green functions (DFT + NEGF), and the properties of SET based on them are discussed.

2. Geometry of fullerene nanojunctions

The geometry of the "Gold – Fullerene – Gold" model nanodevices, the conduction channels of which are fullerene C_{180} and fullerene matryoshkas C_{80}@C_{180}, (C_{20}@C_{80})@C_{180}, located between two gold electrodes, is shown in Fig. 1(a)-(c). The nanodevices under consideration are nanoobjects in the form of endofullerenes placed in a nanogap with a size of ~17.13 Å. The distance from the fullerene surface to the electrodes is ~2.58 Å. The size of the electrodes is ~ 24.47 Å × 24.47 Å and consist of 460 gold atoms. The size of the scattering region of quasiparticles is commensurate with the size of C_{180} molecules (with a diameter of ~ 11.97 Å). The main geometric parameters of the considered nanodevices of the «core – shell» type are shown in Figs. 1(a)-1(c).

Fig. 2 shows the electron densities of fullerene nanodevices. As can be seen, the electron density of endofullerenes C_{80}@C_{180}, (C_{20}@C_{80})@C_{180} significantly exceeds the electron density of fullerene C_{180}. It is obvious

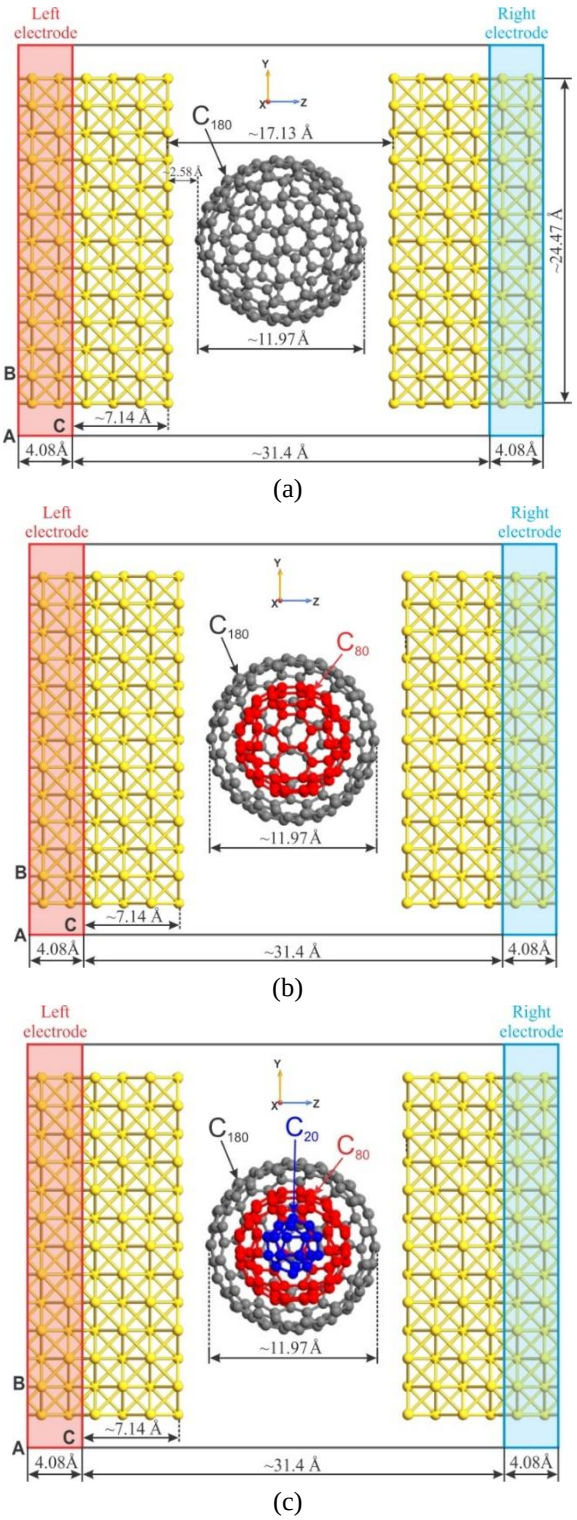

Fig. 1 The geometry of nanodevices: (a) Au–C_{180}–Au; (b) Au–C_{80}@C_{180}–Au; (c) Au–(C_{20}@C_{80})@C_{180}–Au

that this is the contribution of the electrons of encapsulated fullerenes with small diameters. The electron density in the center of endofullerene nanodevices is almost twice that of a fullerene device. For example, in a C_{80}@C_{180}- device, the electron density reaches up to ~710 Å^{-3}, and in (C_{20}@C_{80})@C_{180} it is ~850 Å^{-3}, when in a C_{180}- device it is – 420 Å^{-3} (Fig. 3).

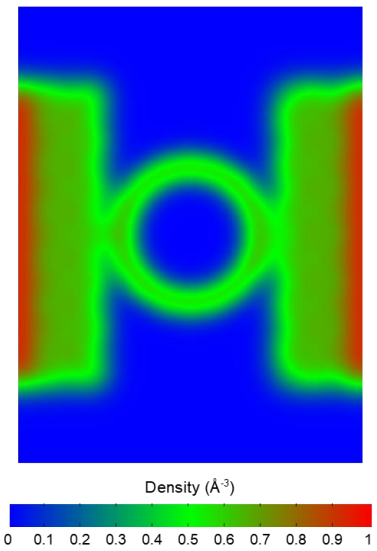

(a)

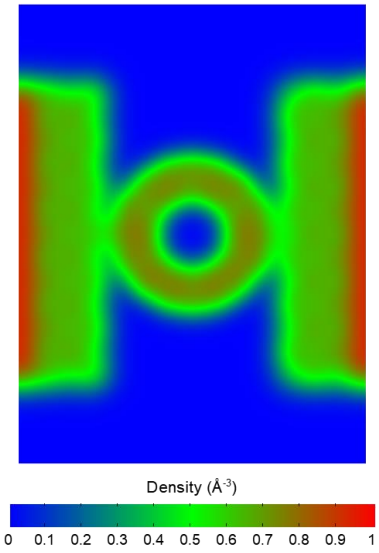

(b)

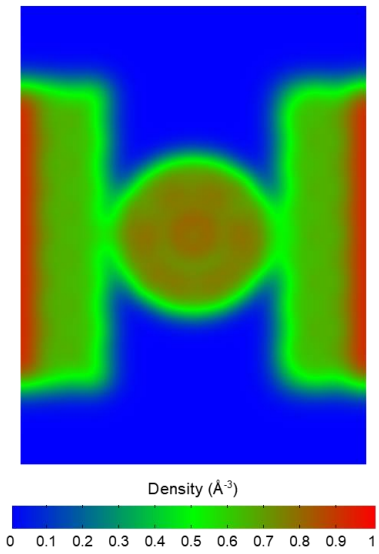

(c)

Fig. 2 Electronic densities of nanodevices: (a) Au–C_{180}–Au; (b) Au–C_{80}@C_{180}–Au; (c) Au–(C_{20}@C_{80})@C_{180}–Au

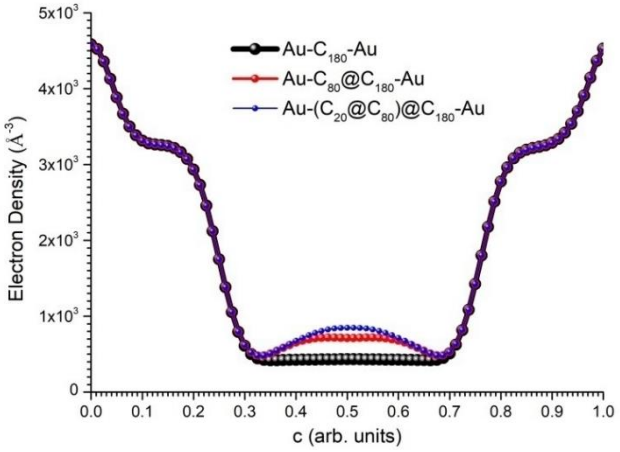

Fig. 3 Distribution of the electron density of nanodevices along the C-axis

3. Fundamental equations

The procedure for optimizing the geometry of fullerene nanodevices and describing the interatomic interaction was carried out within the framework of the DFT, the generalized gradient approximation GGA-PBE (Perdew *et al*. 1996, Ferre *et al*. 2016) was used as an exchange-correlation functional, which allows us to describe such structures most accurately. When optimizing the nanostructures, the parameters of the atomic configuration were relaxed until the forces on all the atoms of the molecule became less than the specified threshold value of 0.05 eV/Å.

Computer-generated simulation of the electrical characteristics of the nanojunction was carried out within the framework of the density functional theory in combination with the method NEGF and using the local-density approximation (LDA) (Smidstrup *et al.* 2017, Brandbyge *et al.* 2002, Stokbro 2008, Ganjia *et al.* 2008). Modeling of the electric transport properties of the nanojunction is realized in the Atomistix ToolKit with Virtual NanoLab program. (Fundamental equations of this method are described in detail in our previous works (Sergeyev 2020c, Sergeyev and Shunkeyev 2018)). To calculate the current-voltage characteristic (CVC) and differential conductivity, the transmission spectrum (function) $T(\varepsilon)$ of the considered nanojunction is first determined:

$$T(\varepsilon) = tr[\Gamma^L G \Gamma^R G^\dagger] = tr[\Gamma^R G \Gamma^L G^\dagger], \quad (1)$$

where $\boldsymbol{\Gamma^{L(R)}(\varepsilon)}$ is the broadening matrix (the broadening function) of the left (right) electrode, $\boldsymbol{G(\varepsilon)}$, $\boldsymbol{G^\dagger(\varepsilon)}$ are the retarded and advanced Green functions, $\boldsymbol{\varepsilon}$ is the energy. The CVC of the nanostructure is calculated on the basis of the well-known Landauer equation, which indicates the fundamental relationship of the electric current with the transmission spectrum (Landauer 1970):

$$I(V_L, V_R, T_L, T_R) = \frac{2e}{h}\int_{-\infty}^{+\infty} T(\varepsilon)\left[f\left(\frac{\varepsilon-\mu_R}{k_B T_R}\right) - f\left(\frac{\varepsilon-\mu_L}{k_B T_L}\right)\right] d\varepsilon, \quad (2)$$

where $\boldsymbol{e}$ is electron charge, $\boldsymbol{h}$ is Planck's constant, $\boldsymbol{f(\varepsilon)}$ is Fermi energy distribution function of quasiparticles, $\boldsymbol{k_B}$ is the Boltzmann's constant, T_L , $\boldsymbol{T_R}$ are current temperatures and $\boldsymbol{\mu_R}$, $\boldsymbol{\mu_L}$ are electrochemical potentials of the right and left electrodes.

The differential conductivity of the nanostructure was obtained by calculating a self-consistent current at a number of applied biases V_{bias}^1, V_{bias}^2, and performing numerical differentiation:

$$\sigma(V_{bias}, T_L, T_R) = \frac{I(V_{bias}^1, T_L, T_R) - I(V_{bias}^2, T_L, T_R)}{V_{bias}^1 - V_{bias}^2}. \qquad (3)$$

4. Results and discussions

The evolution of the transmission spectrum of fullerene nanodevices with an increase in the bias voltage from -3 V to 3 V is shown in Fig. 4. The bias voltage increased in increments of 0.3 V. The transmission spectrum of fullerenes uses the energies of the molecular orbit for the applied bias voltage to determine at which energies the electron transport will be strongest. The spectra were constructed for HOMO (Highest Occupied Molecular Orbital) – LUMO (Lowest Unoccupied Molecular Orbital) energies relative to the Fermi level energy, which was considered as zero energy ($\boldsymbol{\varepsilon_F = 0}$). Fig. 4 shows various applied voltages with different color fills (from the color black (-3 V) to the color army green (3 V)).

With an increase in the value of the bias voltage, the intensity of the transmission spectrum also increases. It is known that the greater the number of peaks in the transmission spectrum, the higher the indicators of the transport of quasiparticles through the nanodevice consideration. At positive energy, the intensity of the transmission spectrum of the C_{180}-nanodevice nanodevice energy peak prevails relative to the intensity at negative energy. Maximum peak $T(\varepsilon)$ observed at energy 1.35 eV. The transmission spectrum of the C_{180}-nanodevice shows that a noticeable weakening of the conductivity occurs near the Fermi energy. In the energy range of -0.45÷0.45 eV, the C_{180} molecule does not pass quasiparticles, forming a HOMO-LUMO gap equal to 0.9 eV, however, when small-sized fullerenes C_{80} and C_{20} are introduced into C_{180}, this gap disappears and a series of peak resonant structures appear on the transmission spectrum of C_{80}@C_{180}-, (C_{20}@C_{80})@C_{180}-nanodevices. In the energy range of -0.45÷0.45 eV, the C_{180} molecule does not pass quasiparticles, forming a HOMO-LUMO gap equal to 0.9 eV, however, when small-sized fullerenes C_{80} and C_{20} are introduced into C_{180}, this gap disappears and a series of peak resonant structures appear on the transmission spectrum of C_{80}@C_{180}-, (C_{20}@C_{80})@C_{180}- nanodevices. Also, in the energy range of -1.81÷0.89eV, no current flows through the C_{180}-nanodevice ($T(\varepsilon) \sim 0$). C_{80}@C_{180}-, (C_{20}@C_{80})@C_{180}- nanodevices are a resonant tunnel structure, so their transmission spectra have complex resonant peaks (Figs. 4(b) and 4(c)). As can be seen, the introduction of C_{20} and C_{80} molecules into the C_{180} fullerene cavity simultaneously enhances the resonance effect, which leads to an increase in the resonance peaks on the spectrum.

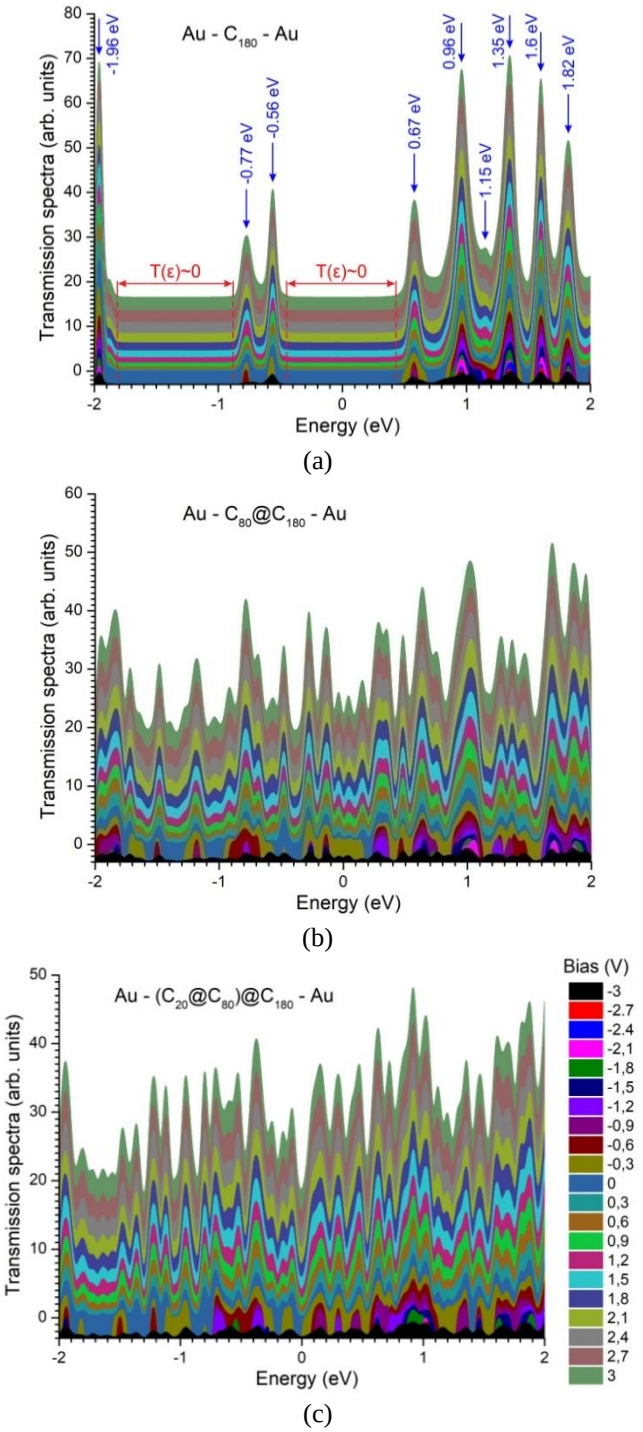

Fig. 4 Evolution of the transmission spectrum of nanodevices with an increase in the bias voltage from -3V to 3V: (a) Au–C_{180}–Au; (b) Au–C_{80}@C_{180}–Au; (c) Au–(C_{20}@C_{80})@C_{180}–Au

Given that the conductivity is directly proportional to the transmission, it can be concluded that a current flows well through the endofullerenes C_{80}@C_{180}, (C_{20}@C_{80})@C_{180}, less than C_{180}.

The results of modeling the CVC and differential conductivity are shown in Figs. 5 and 6, respectively. (CVC and the differential conductivity of the nanostructures under consideration are calculated using the Eqs. (2) and (3). The

CVC of C_{180}- nanodevice has distinct stepped sections – "Coulomb staircase". These step structures arise with the period $\Delta V = \frac{e}{C_{min}}$ (there C_{min} – junction capacitance with lower conductivity (with greater resistance). The appearance of a stepped Coulomb staircase on the CVC is explained by the existence of a spatial correlation of the acts of tunneling of individual electrons in a nanodevice with two tunnel transitions formed in the area where gold electrodes are in contact with a fullerene molecule (Fig. 1). For the interpretation of the operation of such nanojunctions, the single-electron nanocapacitor-recharging model is used. From the theoretical consideration of electron transport in such nanojunction, when a charge enters a quantum dot (a fullerene molecule), a charge is established on the polarizable surface of the nanostructure, causing a powerful Coulomb attraction between two closely spaced charges located at the electrode-molecule interface. After that, there is a restriction of electron transport – a Coulomb blockade, i.e., the total charge blocks the input of one elementary charge into the C_{180} molecule and the output of one elementary charge from the C_{180} molecule. However, with an increase in the bias voltage, an electron is removed from the molecule, and another electron replaces its place. In the voltage range of -0.37÷0.37 V, electronic transport is impossible due to the Coulomb blockade and the current in the C_{180} junction is zero. At first glance, it seems that the blocking of electrons occurs in a relatively wide voltage range from -0.84÷0.84 V, but this is not the case. As can be seen from Fig. 5, a small current with an amplitude of ~0.3 μA flows in the voltage intervals [-0.84; -0.37] and [0.37; 0.84].

Indistinct (smeared) "Coulomb staircase" are observed on the CVC of C_{80}@C_{180}-, (C_{20}@C_{80})@C_{180}- nanojunction. Probably, this is due to a decrease in the Coulomb energy $E_c = \frac{e^2}{2C}$ due to an increase in the intrinsic electrical capacity of the molecules C_{80}@C_{180}, (C_{20}@C_{80})@C_{180}. Assuming that the shape of the fullerene is spherical, to estimate the intrinsic electrical capacity of the fullerene molecule C_{180}, we use the formula of the electrical capacity of a spherical capacitor: (4)

$$C = 4\pi\varepsilon_0 r \qquad (4)$$

where $\varepsilon_0 = 8.85 \cdot 10^{-12}$ F/m, $r = r_{C_{180}} \approx 5.985$ Å is radius of the C_{180} fullerene molecule. The calculated value of the capacity of the C_{180} molecule (according to the formula (4)) is $6.66 \cdot 10^{-20}$F. To calculate the intrinsic electrical capacity of C_{80}@C_{180}, (C_{20}@C_{80})@C_{180} molecules, we use the formula for the electrical capacity of conducting concentric spheres, assuming the shape of all types of fullerenes to be spherical:

$$C = \frac{4\pi\varepsilon_0 r_1 r_2}{(r_2 - r_1)}, \qquad (5)$$

where $r_2 > r_1$ are radiuses of concentric spheres (radiuses of a fullerene molecule ($r_{C_{80}} \approx 4.118$ Å, $r_{C_{20}} \approx 1.99$ Å). The intrinsic electrical capacity of the C_{80}@C_{180} molecule is $14.69 \cdot 10^{-20}$ F, and of the (C_{20}@C_{80})@C_{180} molecule – ~$12 \cdot 10^{-20}$ F, which is almost twice as much as the electrical capacity of the C_{180} molecule. An increase in the capacity

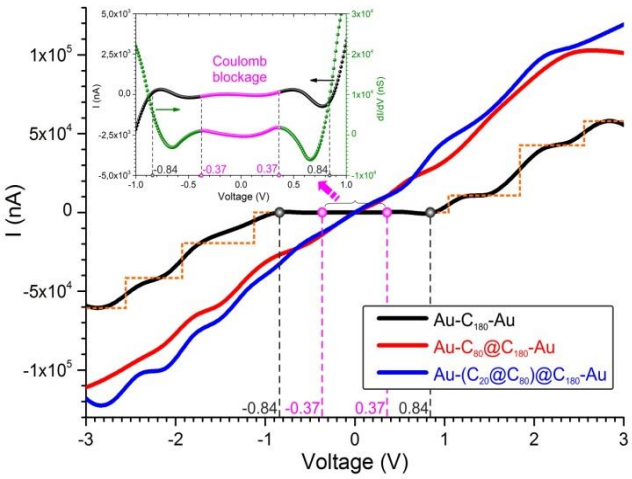

Fig. 5 Current-voltage characteristics of nanodevices (the orange dotted line marks the ideal CVC of the nanocapacitor in the case of the Coulomb blockade effect)

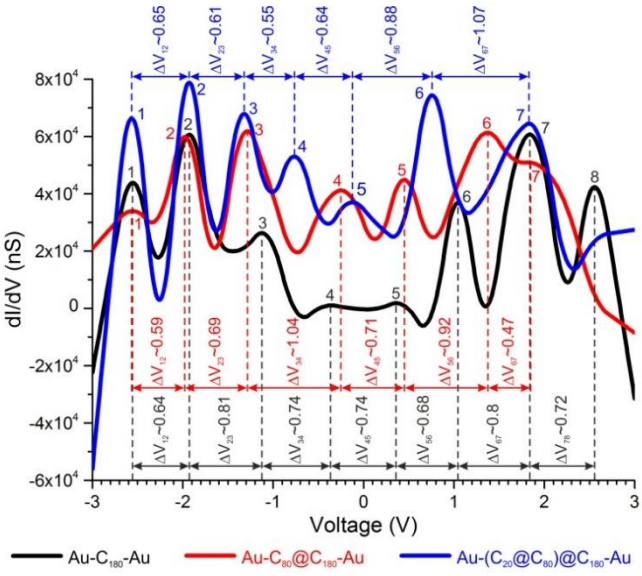

Fig. 6 – *dI/dV* characteristics of nanodevices based on C_{180} molecule

leads to a decrease in the Coulomb energy and an increase in the influence of thermal fluctuations.

Coulomb ladders of the CVC on the *dI/dV* spectrum are observed in the form of an oscillation with a constant voltage period ΔV (Fig. 6). On the *dI/dV* spectrum of the C_{180} nanojunction in the voltage range from -3 V to 3 V, we observe 8 distinct peak structures. The ΔV value varies from 0.64 V (ΔV_{12}) to 0.81 V (ΔV_{23}). Here, the ΔV period indices show the corresponding peaks of the *dI/dV* spectrum that determine its value. The average value of the period C_{180} is the nanojunction $\Delta V_{a.v.} \approx 0.73$ B. A noticeable deviation ΔV from the mean value $\Delta V_{a.v.}$ is observed when it is negative V_{bias} between peaks 2 and 3 ($\Delta V_{23} \approx$ 0.81V), when it is positive V_{bias} between peaks 6 and 7 ($\Delta V_{67} \approx 0.8$V). The voltage period determines the width of the Coulomb step in the CVC, i.e., the larger ΔV, the wider the Coulomb step in the CVC. The deviation (blurring)

from the ideal rectangular shape of the Coulomb staircase on the CVC appears itself on the *dI/dV* spectrum as an increase in the width of the peak. (Note that the narrower the peaks of the *dI/dV* spectrum, the more distinct the shape of the Coulomb staircase on the CVC). For example, the blurring of the CVC in the range ΔV_{67} appears stronger, where the width of the seventh peak is 0.75 V.

The differential conductivity of the C_{80}@C_{180}-nanojunction has 7 peaks, the value of the voltage period varies from 0.47V to 1.04V. There is a significant spread in the value ΔV. The average value of the period C_{80}@C_{180} is the nanojunction $\Delta V_{a.v.} \approx 0.74$V. One of the features of the *dI/dV* spectrum is the merging of the sixth and seventh peaks, which leads to a significant reduction of the period to $\Delta V_{67} \approx 0.47$V. Note that the period spread is also observed between the third and fourth peaks $\Delta V_{34} \approx 1.04$V.

We observe a similar behavior of the differential conductivity (C_{20}@C_{80})@C_{180}, where there is a significant spread of the period value over the voltage from 0.55 V to 1.07 V. What is more, a strong spread ΔV occurs at a positive bias voltage, and at a negative bias voltage, the period ΔV is more stable, and on average is ~ 0.61 V. As can be seen, there is a significant increase in the period $\Delta V_{67} \approx 1.07$V between the sixth and seventh peaks of the *dI/dV* spectrum. This change in the CVC is reflected by a strong blurring of the Coulomb step, which shows the weak influence of Coulomb effects in this voltage range. In the *dI/dV* spectrum of C_{80}@C_{180}- and (C_{20}@C_{80})@C_{180}-nanojunctions the width of the peak is narrower at negative V_{bias}, than at positive V_{bias}, and accordingly, the CVC at negative V_{bias} appear more distinctly Coulomb steps than at positive V_{bias}.

According to the results of the calculations, fullerene nanojunctions have two ballistic channels. This means that they have a conductivity value of $2G_0$ (here G_0 is the conductance quantum).

For comparison, it should be noted that four (Nasri 2018) and six Coulomb features are observed in the dI/dV spectrum of C_{60}-nanojunctions with Pt- and Au-electrodes (Sergeyev *et al*. 2021). This shows that single-electron transport occurs faster in the considered fullerene nanojunctions of the «core-shell» type than in C_{60}-nanodevices with Pt-, Au- and graphene electrodes.

Consider the operation of the charge stability diagram (Coulomb rhombuses (diamonds)) SET based on C_{180}, C_{80}@C_{180} and (C_{20}@C_{80})@C_{180} (Fig. 6). SET, represents the molecular structures considered in Fig. 1, with the addition of a control gate electrode to the lower part of the device - gate. The gate is separated from the main structure of the SET by a thin layer of dielectric ~3.7 A. Dielectric constant of the dielectric is $10\varepsilon_0$. The distance from fullerenes to the dielectric surface is ~1.8A. It is known that the transport of a charge in a SET occurs when it overcomes the Coulomb blockade region. One of the options for the electron to overcome this bandgap is to supply sufficient charging energy by adjusting the gate and source-drain potentials. As the gate voltage changes, the HOMO and LUMO levels shift. When a positive gate voltage is applied, the LUMO level shifts below the Fermi level of the electrode and subsequently attracts an electron, which is responsible for

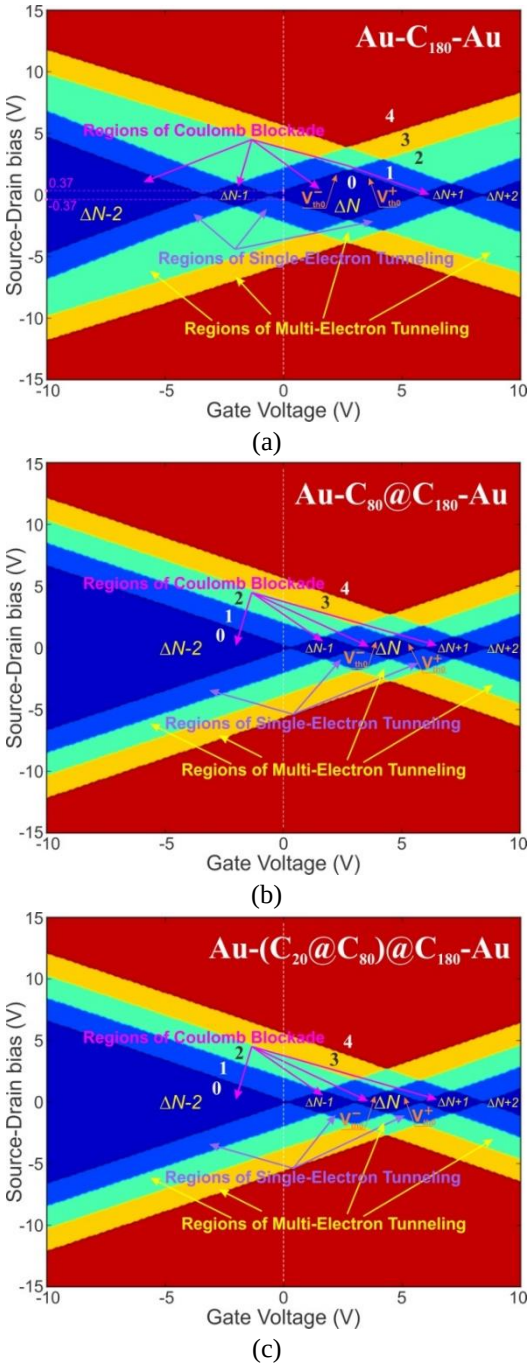

Fig. 7 Charge stability diagrams for (a) C_{180}-, (b) C_{80}@C_{180}-, and (c) (C_{20}@C_{80})@C_{180}-based SETs. The number of charge states in the bias window for given bias potentials is given by the specific color. The color map is: blue (0), light blue (1), green (2), yellow (3), red (4)

the negative charge of the molecular islet, whereas with a negative gate voltage, the HOMO level shifts above the Fermi electrode level, as a result, the electron escapes from the island and charges it to a positive one. For the specified values of the source-drain and gate bias voltage, the number of molecular energy levels inside the window is given by color codes (Figs. 7(a)-7(c)). The equilibrium value of the number of excess electrons ΔN is indicated inside each Coulomb diamond. The area of the Coulomb blockade is

Table 1 Parameters of the central Coulomb diamond

	V_{SDmin}	V_{SDmax}	ΔV_{SD}	V_{Gmin}	V_{Gmax}	ΔV_G	Diamond Area
C_{180}	-2.041	2.079	4.12	-0.618	5.71	6.328	13.036
C_{80}@ C_{180}	0.973	-0.896	1.869	3.09	5.914	9.004	8.414
(C_{20}@C_{80})@ C_{180}	0.973	-0.935	1.908	2.997	5.833	8.83	8.424

represented in dark blue and is indicated by the number 0. If the SET operating point is located inside this Coulomb rhombus, where there is no energy level to support electronic transport, then the transport of electrons through the transistor is impossible. Single-electron tunneling in transistors occurs in the area represented by a light blue color and marked with the number 1. The inclined lines between these regions correspond to the threshold voltages at which SET opens and current transport becomes possible, i.e., single-electron transport is blocked until the voltage reaches the threshold value V_{th0}^{-} or V_{th0}^{+} (Fig. 7). Behind the dark blue (Coulomb blockade region) and light blue regions (single-electron tunneling region), multi-electron tunneling occurs.

The optimal value of the gate voltage V_G for controlling the SET modes based on C_{180}, C_{80}@C_{180} and (C_{20}@C_{80}) @C_{180} is in the intervals of -3.41÷8.42 V, 0.28÷8.6 V and 0.22÷8.43 V, respectively. Outside the specified interval, relatively high drain-source voltages must be applied to exit the Coulomb blockade mode V_{SD}. Note that the $V_{SD}(V_G)$ dependence has special points where a negligibly small V_{SD} voltage is required to exit the Coulomb blockade mode into the single-electron tunneling mode, for example, for C_{180}-SET these points are V_G ~ -3.41 V; -0.5 V; 5.7 V; 8.43 V, for C_{80}@C_{180}-SET – V_G ~ 0.28 V; 3.1 V; 5.9 V; 8.6 V and for (C_{20}@C_{80})@C_{180}-SET – V_G ~ 0.22 V; 3.02 V; 5.82 V; 8.43 V.

At zero gate voltage, the data of the stability diagram of fullerene transitions correlate well with the data of the *IV*- and *dI/dV*-characteristics of fullerene transitions. For example, the diagram shows that the Coulomb blockade effect of the C_{180}-junction occurs in the voltage range -0.37÷0.37 V, and in endofullerene transitions, the blocking of electron transfer is observed in the range ~ -0.1÷0.1 V.

The ranges of the Coulomb blockade associated with the central Coulomb diamond, as well as their areas extracted from Fig. 7, are presented in Table 1. The areas of Coulomb diamonds are calculated using the formula for determining the area of the rhombus: Diamond Area $= \frac{(\Delta V_{SD} \cdot \Delta V_G)}{2}$. Maximum and minimum values of the drain-source bias voltage of C_{180}-, C_{80}@C_{180}-, (C_{20}@C_{80})@C_{180}-nano-transistors are manifested at a gate voltage of 2.74 V, 4.5 V and 4.41 V, respectively. A comparative study of the table shows that the area of the central diamond of the Coulomb blockade of the C_{180} molecule is 1.5 times larger than other molecules.

These results can be useful in the design of the SET, since a decrease in the area of the Coulomb diamond in the stability diagram can lead to smaller fluctuations, so, current fluctuations as a limiter of the SET operation are reduced and, therefore, the SET can operate at higher speeds.

5. Conclusions

Thus, in this framework the electric transport properties (transmission spectra, CVC, differential conductivity, electron density) of the model nanojunctions "Au–C_{180}–Au", "Au–C_{80}@C_{180}–Au" and "Au–(C_{20}@C_{80})@C_{180}–Au" were studied within the framework of DFT + NEGF. It is shown that the matryoshka combination of fullerenes with different diameters leads to a significant change in their electrical properties. The following results were obtained:

• An increase in the number of resonant peaks of the transmission spectrum was revealed when C_{20}, C_{80} fullerenes of small radius were introduced into the C_{180} fullerene cavity.

• In the range of -0.45÷0.45 eV, a HOMO–LUMO gap is formed in the transmission spectrum of the "Au–C_{180}-Au" nanojunction, its width is 0.9 eV. In the case of the introduction of small-sized fullerenes into C_{180}, though, this gap disappears and a series of peak resonant structures appear on the transmission spectrum of C_{80}@C_{180}-, (C_{20}@C_{80})@C_{180}-nanojunctions.

• It is shown that distinct step structures of Coulomb origin appear on the CVC of the C_{180}- nanojunctions. On CVC of C_{80}@C_{180}-, (C_{20}@C_{80})@C_{180}-nanojunctions these step structures are «smeared» due to the weakening of the Coulomb energy associated with an increase in the intrinsic electrical capacities of the molecules.

• 8 peak structures of Coulomb origin with a period of 0.73 V appear on the *dI/dV* spectrum of the C_{180}-nanojunction, and 7 peak structures with periods of 0.74 V and 0.61 V, respectively, appear on the spectrum of C_{80}@C_{180}-, (C_{20}@C_{80})@C_{180}-nanojunctions, respectively.

• It is shown that the output of the C_{180}-SET from the Coulomb blockade mode requires a large source-drain voltage compared to transistors based on C_{80}@C_{180}-, (C_{20}@C_{80})@C_{180}- nanojunctions.

• Reducing the area of the Coulomb diamond on the charge stability diagram C_{80}@C_{180}-, (C_{20}@C_{80})@C_{180}-S*Et al*lows you to increase the performance of integrated circuits based on them.

The simulation results obtained in this work can be useful in creating high-speed single-electron nanodevices.

Acknowledgements

This research is funded by the Science Committee of the Ministry of Education and Science of the Republic of Kazakhstan (Grant No AP08052562)

References

Akasaka, T., Nagase, S. (2002), *Endofullerenes (A New Family of Carbon Clusters)*, Springer, Netherlands.

Artyukh, A.A. and Chernozatonskii L.A. (2020), "Simulation of the formation and mechanical properties of layered structures with polymerized fullerene-graphene components", *JETP Lett*., **111**(2), 109-115. https://doi.org/10.31857/S0370274X20020083.

Averin, D.V. and Likharev, K.K. (1986), "Coulomb blockade of single-electron tunneling, and coherent oscillations in small tunnel junctions", *J. Low Temp. Phys.*, **62**(3), 345-373. https://doi.org/10.1007/BF00683469.

Bal, M., Long, J., Zhao, R., Wang, H., Park, S., McRae, C.R.H., Zhao, T., Lake, R., Monarkha, V., Simbierowicz, S., Frolov, D., Pilipenko, R., Zorzetti, S., Romanenko, A., Liu, C.H., McDermott, R. and Pappas, D. (2021), "Overlap junctions for superconducting quantum electronics and amplifiers", *Appl. Phys. Lett.*, **118**(11), 112601. https://doi.org/10.1063/5.0048621.

Brandbyge, M., Mozos, J.L., Ordejon, P., Taylor, J. and Stokbro, K. (2002), "Density-functional method for nonequilibrium electron transport", *Phys. Rev. B*, **65**(16), 165401. https://doi.org/10.1103/PhysRevB.65.165401.

Brandbyge, M., Mozos, J.L., Ordejon, P., Taylor, J. and Stokbro, K. (2002), "Density-functional method for nonequilibrium electron transport", *Phys. Rev. B*, **65**(16), 165401. https://doi.org/10.1103/PhysRevB.65.165401.

Burroughs, C.J., Benz, S.P., Harvey, T.E. and Hamilton, C.A. (1999), "1 Volt DC Programmable Josephson Voltage Standard System", *IEEE T Appl Superconduct.*, **9**(2), 4145-4148. https://doi.org/10.1109/77.783938.

Cardenas-Jiron, G.I., Borges-Martinez, M., Sikorski, E. and Baruah, T. (2017), "excited states of light-harvesting systems based on fullerene/graphene oxide and porphyrin/smaragdyrin", *J. Phys. Chem. C*, **121**(9), 4859-4872. https://doi.org/10.1021/acs.jpcc.6b12452.

Castro Neto, A.H., Guinea, F., Peres, N.M.R., Novoselov, K.S. and Geim, A.K. (2009), "The electronic properties of graphene", *Rev. Mod. Phys*., **81**(1), 109-162. https://doi.org/10.1103/RevModPhys.81.109.

Cattaneo, M., Giorgi, G., Maniscalco, S., Paraoanu, G. and Zambrini, R. (2021), "Bath-induced collective phenomena on superconducting qubits: Synchronization, subradiance, and entanglement generation", *Annalen der Physik*, **533**(5), 2100038. https://doi.org/10.1002/andp.202100038.

Ceron, M.R., Zhan, C., Campbell, P.G., Freyman, M.C., Santoyo, C., Echegoyen, L. and Biener, M.M. (2019), "Integration of fullerenes as electron-acceptors in 3d graphene networks: Enhanced charge transfer and stability through molecular design", *ACS Appl. Mater. Interf.*, **14**(11), 28818-28822. https://doi.org/10.1021/acsami.9b06681.

Champagne, A.R., Pasupathy, A.N. and Ralph, D.C. (2005), "Mechanically adjustable and electrically gated single-molecule transistors", *Nano Letters*, **5**(2), 305-308. https://doi.org/10.1021/nl0480619.

Chen, R., Lin, C., Yu, H., Tang, Y., Song, C., Yuwen, L. and Huang, W. (2016), "Templating C_{60} on MoS_2 nanosheets for 2d hybrid van der waals p-n nanoheterojunctions", *Chem. Mater.*, **28**(12), 4300-4306. https://doi.org/10.1021/acs.chemmater.6b01115.

Chuan, M.W., Lau, J.Y., Wong, K.L., Hamzah, A., Alias, N.E., Lim, C.S. and Tan, M.L.P. (2021), "Low-dimensional modelling of n-type doped silicene and its carrier transport properties for nanoelectronic applications", *Adv. Nano Res.*, **10**(5), 415-422. https://doi.org/10.12989/anr.2021.10.5.415.

Chuan, M.W., Wong, K.L., Hamzah, A., Rusli, S., Alias, N.E., Lim, C.S. and Tan, M.L.P. (2021), "Device modelling and performance analysis of two-dimensional $AlSi_3$ ballistic nanotransistor", *Adv. Nano Res.*, **10**(1), 91-99. https://doi.org/10.12989/anr.2021.10.1.091.

Cuevas, J.C. and Scheer, E. (2017), *Molecular Electronics (An Introduction to Theory and Experiment)*, World Scientific Publishing Co. Pte. Ltd., New Jersey, U.S.A.

Dalessandro R.B., Bocchi, M., Rossi, V. and Martini L.F. (2007), "Test results on 500 kva-classmgb_2-based fault current limiter prototypes", *IEEE T Appl. Superconduct.*, **17**(2), 1776-1779. https://doi.org/10.1109/TASC.2007.899034.

Daqiq, R. (2021), "Spin-filter devices based on resonant magnetic tunnel junctions", *J. Electron. Mater.*, **50**(7), 3930-3936. https://doi.org/10.1007/s11664-021-08892-x.

Davis, N., Rudge, S.L. and Kosov, D.S. (2021), "Electronic statistics on demand: Bunching, antibunching, positive, and negative correlations in a molecular spin valve", *Phys. Rev. B*, **103**(20), 205408. https://doi.org/10.1103/PhysRevB.103.205408.

Devi J.M. (2019), "Simulation of graphene-fullerene nanohybrid structure", *Bull. Mater. Sci.*, **42**(2), 75. https://doi.org/10.1007/s12034-019-1753-0.

Dragoman, M., Dinescu, A. and Dragoman, D. (2019), "2D materials nanoelectronics: Mew concepts, fabrication, characterization from microwaves up to optical spectrum", *Phys. Status Solidi A*, **216**(8) 1800724. https://doi.org/10.1002/pssa.201800724.

Dragoman, M. and Dragoman, D. (2017), *2D Nanoelectronics: Physics and Devices of Atomically Thin Materials*, Springer International Publishing, Cham, Switzerland.

Eletskii, A.V. (1997), "Carbon nanotubes", *Phys. Usp*., **40**, 899-924. https://doi.org/10.3367/UFNr.0167.199709b.0945.

Faley, M. I., Poppe, U., Borkowski, R. D., Schiek, M., Boers, F., Chocholacs, H., Dammers, J., Eich, E., Shah, N.J., Ermakov, A.B., Slobodchikov, V.Yu., Maslennikov, Yu, V. and Koshelets, V.P. (2012), "Magnetoencephalography using a Multilayer hight C DC SQUID Magnetometer", *Phys. Proced.*, **36**, 66-71. https://doi.org/10.1016/j.phpro.2012.06.131.

Ferre, N., Filatov, M. and Huix-Rotllant M. (2016), *Density-Functional Methods for Excited States*, Springer International Publishing, Cham, Switzerland.

Fried, J.P., Bian, X., Swett, J.L., Kravchenko, I.I., Briggs, G.A.D. and Mol, J.A. (2020), "Large amplitude charge noise and random telegraph fluctuations in room-temperature graphene single-electron transistors", *Nanoscale*, **12**(2), 871-876. https://doi.org/10.1039/c9nr08574b.

Ganjia, M.D. and Nourozi, F. (2008), "Density functional non-equilibrium Green's function (DFT-NEGF) study of the smallest nano-molecular switch", *Physica E*, **40**(7,) 2606-2613. https://doi.org/10.1016/j.physe.2007.09.123.

Gaurav, K., SanthiBhushan, B., Ray, S. and Srivastava, A. (2019), "Acridinium based organic molecular single-electron transistor for high performance switching applications", *IEEE T Nanotechnol.*, **18**, 1148-1155. https://doi.org/10.1109/TNANO.2019.2945995.

Gehring, P., Harzheim, A., Spièce, J., Sheng, Y., Rogers, G., Evangeli, C. and Mol, J.A. (2017), "Field-effect control of graphene-fullerene thermoelectric nanodevices", *Nano Lett.*, **17**(11), 7055-7061. https://doi.org/10.1021/acs.nanolett.7b03736.

Geim, A.K. (2009), "Graphene: Status and prospects", *Science*, **324**(5934), 1530-1534. https://doi.org/10.1126/science.1158877.

Geim, A.K. and Grigorieva, I.V. (2013), "Van der Waals heterostructures", *Nature*, **499**(25), 419-425. https://doi.org/10.1038/nature12385.

Gyanchandani, N., Pawar, S., Maheshwary, P. and Nemade, K. (2021), "Comprehensive study of spin field effect transistors with co-graphene ferromagnetic contacts", *J. Magnetism and Magnetic Mater.*, **517**, 167410. https://doi.org/ 10.1016/j.jmmm.2020.167410.

Hirohata, A., Yamada, K., Nakatani, Y., Prejbeanu, I.L., Dieny,

B., Pirro, P. and Hillebrands, B. (2020), "Review on spintronics: Principles and device applications", *J. Magnetism Magnetic Mater.*, **509**, 166711. https://doi.org/10.1016/j.jmmm.2020.166711.

Huang, W.Q., Liu, S.R., Peng, H.Y., Li, X. and & Huang, Z.M. (2020), "Synthesis of new silicene structure and its energy band properties", *Chinese Phys. B*, **29**(8), 084202. https://doi.org/10.1088/1674-1056/ab942c.

Iijima, S. (1991), "Helical microtubules of graphitic carbon", *Nature*, **354**(6348), 56-58. https://doi.org/10.1038/354056a0.

Kalashnikov, K., Artanov, A.A., de Lange, G. and Koshelets, V.P. (2018), "Investigation of the harmonic mixer and low-frequency converter regimes in a superconducting tunnel junction", *IEEE T Appl. Superconduct.*, **28**(4), 2400105. https://doi.org/10.1109/TASC.2018.2803043.

Kang, A.K., Zandi, M.H. and Gorji, N.E. (2019), "Simulation analysis of graphene contacted perovskite solar cells using SCAPS-1D", *Optical Quant. Electron.*, **51**(4), 91. https://doi.org/10.1007/s11082-019-1802-3.

Khadem Hosseini, V., Ahmadi, M.T. and Ismail, R. (2018), "Analysis and modeling of fullerene single-electron transistor based on quantum dot arrays at room temperature", *J. Electron. Mater.*, **47**(8), 4799-4806. https://doi.org/10.1007/s11664-018-6366-7.

Khademhosseini, V., Dideban, D. and Ahmadi, M. (2021), "The current analysis of a single-electron transistor based on double grapheme nanoscroll island", *Solid State Commun.*, **327**(7), 114234. https://doi.org/10.1016/j.ssc.2021.114234.

Kharlamova, M.V. (2013), "Electronic properties of pristine and modified single-walled carbon nanotubes", *Phys. Usp.*, **56**(11), 1047-1073. https://doi.org/10.3367/UFNe.0183.201311a.1145.

Kiraly, B., Liu, X., Wang, L., Zhang, Zh., Mannix, A.J., Fisher, B.L., Yakobson, B.I. and Hersam, M.C., Guisinger, N.P. (2019), "Borophene synthesis on Au(111)", *ACS Nano*, **13**(4), 3816-3822. https://doi.org/10.1021/acsnano.8b09339.

Koh, W., Moon, H.S., Lee, S.G., Choi, J.I. and Jang, S.S. (2014), "A first-principles study of lithium adsorption on a graphene-fullerene nanohybrid system", *ChemPhysChem*, **16**(4), 789-795. https://doi.org/10.1002/cphc.201402675.

Kornev, V.K., Kolotinskiy, N.V., Sharafiev, A.V., Soloviev, I.I. and Mukhanov, O.A. "Broadband active electrically small superconductor antennas", *Supercond. Sci. Technol.*, **30**(10), 103001. https://doi.org/10.1088/1361-6668/aa7a52/

Kroto, H.W., Heath, J.R., O'Brien, S.C., Curl, R.F. and Smalley, R.E. (1985), "C_{60}: Buckminsterfullerene", *Nature*, **318**(6042), 162-163. https://doi.org/10.1038/318162a0.

Kumar, B.R. (2018), "Investigation on mechanical vibration of double-walled carbon nanotubes with inter-tube Van der waals forces", *Adv. Nano Res.*, **6**(2), 135-145. https://doi.org/10.12989/anr.2018.6.2.135.

Landauer, R. (1970), "Electrical resistance of disordered one-dimensional lattices", *Philos. Mag.*, **21**(172), 863-867. https://doi.org/10.1080/14786437008238472.

Lee, K., Chakram, S., Kim, S., Mujid, F., Ray, A., Gao, H., Park, C., Zhong, Y., Muller, D., Schuster, D. and Park, J. (2019), "Two-dimensional material tunnel barrier for josephson junctions and superconducting qubits", *Nano Lett.*, **19**(11), 8287-8293. https://doi.org/10.1021/acs.nanolett.9b03886.

Likharev, K.K. (2012), "Superconductor digital electronics", *Physica C.*, **482**, 6-18. https://doi.org/ 10.1016/j.physc.2012.05.016.

Likharev, K.K. (1999), "Single-electron devices and their applications", *Proceedings of the IEEE*, **87**(4), 606-632. https://doi.org/10.1109/5.752518.

Macha P., Oelsner G., Reiner J.M., Marthaler M., Andre S., Schon G., Hubner U., Meyer H.G., Il'ichev E., Ustinov A.V. (2014), "Implementation of a quantum metamaterial using superconducting qubits", *Nature Commun.*, **5**(1), 5146. https://doi.org/ 10.1038/ncomms6146.

Marani, R. and Perri, A.G. (2017), "An approach to model the temperature effects on I-V characteristics of CNTFETs", *Adv. Nano Res.*, **5**(1), 61-67. https://doi.org/10.12989/anr.2017.5.1.061.

Martini, L., Arcos, I., Bocchi, M., Brambilla, R., Dalessandro, R., Frigerio, A. and Rossi, V. (2006), "Resistive fault current limiter prototypes: mechanical and electrical analyses", *J. Phys. Conf. Ser.*, **43**(226), 925-928. https://doi.org/10.1088/1742-6596/43/1/226.

Miao, W., Gao, H., Zhou, K., Zhong, J., Ren, Y., Zhang, W., Shi, S., Delorme, Y. (2021), "Linear and nonlinear flux-flow behaviors in superconducting hot-electron bolometer mixers", *Appl. Phys. Lett.*, **118**(11), 112602. https://doi.org/10.1063/5.0045624.

Montanaro, A., Wei, W., De Fazio, D., Sassi, U., Soavi, G., Aversa, P., Ferrari, A.C., Happy, H., Legagneux, P. and Pallecchi, E. (2021), "Optoelectronic mixing with high-frequency graphene transistors", *Nature Commun.*, **12**(1), 2728. https://doi.org/10.1038/s41467-021-22943-1.

Morozov, S.V, Novoselov, K.S. and Geim, A.K. (2008), "Electronic transport in graphene", *Phys. Usp.*, **51**(7), 744-748. https://doi.org/10.1070/PU2008v051n07ABEH006575.

Mouafo, L.D.N., Godel, F., Simon, L., Dappe, Y., Baaziz, W., Noumbe, U., Lorchat, E., Martin, M., Berciaud, S., Doudin, B., Ersen, O., Dlubak, B., Seneor, P. and Dayen, J.F. (2020), "0D/2D heterostructures vertical single electron transistor", *Adv. Funct. Mater.*, **31**(9), 2008255. https://doi.org/10.1002/adfm.202008255.

Murali, R. (2012), *Graphene Nanoelectronics: From Materials to Circuits*, Springer, New York, USA.

Nakajima, A., Shoji, A., Nagano, K. and Kajihara, J. (2015), "Dependence of memory characteristics of fullerene-containing polymer on the kind of gate metal", *Japanese J. Appl. Phys.*, **54**(10), 100303. https://doi.org/10.7567/jjap.54.100303.

Nasri, A., Boubaker, A., Hafsi, B., Khaldi, W. and Kalboussi, A. (2018), "High-sensitivity sensor using c60-single molecule transistor", *IEEE Sens. J.*, **18**(1), 248-254. https://doi.org/10.1109/jsen.2017.2769803.

Novoselov, K.S., Geim, A.K., Morozov, S.V., Jiang, D., Zhang, Y., Dubonos, S.V., Grigorieva, I.V. and Firsov A.A. (2004), "Electric field effect in atomically thin carbon films", *Science.*, **306**(5696), 666-669. https://doi.org/10.1126/science.1102896.

Park, H., Park, J., Lim, A.K.L., Anderson, E.H., Alivisatos, A.P. and McEuen, P.L. (2000), "Nanomechanical oscillations in a single-C_{60} transistor", *Nature*, **407**(6800), 57-60. https://doi.org/10.1038/35024031.

Pasupathy, A.N., Park, J., Chang, C., Soldatov, A.V., Lebedkin, S., Bialczak, R.C., Grose, J.E., Donev, L.A.K., Sethna, J.P., Ralph, D.C. and McEuen, P.L. (2005), "Vibration-assisted electron tunneling in c_{140} transistors", *Nano Lett.*, **5**(2), 203-207. https://doi.org/10.1021/nl048619c.

Perdew, J.P., Burke, K. and Ernzerhof, M. (1996), "Generalized gradient approximation made simple", *Phys. Rev. Lett.*, **77**(18), 3865-3868. https://doi.org/10.1103/PhysRevLett.77.3865.

Pica, M. and D'Amato, R. (2020), "Chemistry of phosphorene: synthesis, functionalization and biomedical applications in an update review", *Inorganics*, **8**(4), 29. https://doi.org/10.3390/inorganics8040029.

Sahoo, S.K. and Wei, K.H. (2019), "A perspective on recent advances in 2D stanene nanosheets", *Adv. Mater. Interf.*, **6**(18), 1900752. https://doi.org/10.1002/admi.201900752.

Sergeyev, D.M. (2012), "About tunneling of pairs of the cooper pairs through the Josephson junctions in exotic superconductors", *Russ. Phys. J.*, **55**(1), 84-91. https://doi.org/10.1007/s11182-012-9779-4.

Sergeyev, D.M. (2013), "Plasma frequency in Josephson junctions with a non-sinusoidal current-phase relation", *Solid State Phenom.*, **200**, 272-275. https://doi.org/10.4028/www.scientific.net/SSP.200.272.

Sergeyev, D.M. (2018), "Computer simulation of electrical characteristics of a graphene cluster with Stone-Wales defects", *J. Nano Electron. Phys.*, **10**(3), 03018. https://doi.org/10.21272/jnep.10(3).03018.

Sergeyev, D.M. (2020a), "Features of the electrical characteristics of an octagraphene nanotube", *J. Nano Electron. Phys*., **11**(6), 06022. https://doi.org/10.21272/jnep.11(6).06022.

Sergeyev, D.M. (2020b), "Single electron transistor based on endohedral metallofullerenes Me@C_{60} (Me = Li, Na, K)", *J. Nano Electron. Phys*., **12**(3), 03017. https://doi.org/10.21272/jnep.12(3).03017.

Sergeyev, D.M. (2020c), "Specific features of electron transport in a molecular nanodevice containing a nitroamine redox center", *Tech. Phys*., **65**(4), 573-577. https://doi.org/10.1134/S1063784220040180.

Sergeyev, D.M. (2021), "One-dimensional Schottky nanodiode based on telescoping polyprismanes", *Adv. Nano Res.*, **10**(4), 339-347. https://doi.org/10.12989/anr.2021.10.4.339.

Sergeyev, D.M. and Shunkeyev, K. (2018), "Investigation of transport parameters of graphene-based nanostructures", *Russ. Phys. J*., **60**(11), 1938-1945. https://doi.org/10.1007/s11182-018-1306-9.

Sergeyev, D.M. and Duisenova, A.G. (2021), "Electron transport in model quasi-two-dimensional van der waals nanodevices", *Tech. Phys. Lett.*, **47**(4), 375-378. https://doi.org/10.1134/S1063785021040295.

Sergeyev, D.M., Ashikov, N. and Zhanturina, N. (2021), "Electric transport properties of a model nanojunction Graphene-Fullerene C_{60}-Graphene", *Int. J. Nanosci.*, **20**(1), 2150007. https://doi.org/10.1142/S0219581X21500071.

Smidstrup, S., Markussen, T., Vancraeyveld, P., Wellendorff, J., Schneider, J., Gunst, T., Verstichel, B., Stradi, D., Khomyakov, P.A., Vej-Hansen, U.G., Lee. M.E., Chill, S.T., Rasmussen, F., Penazzi, G., Corsetti, F., Ojanperä, A., Jensen, K., Palsgaard, M.L.N., Martinez, U., Blom, A., Brandbyge, M. and Stokbro, K. (2020), "QuantumATK: An integrated platform of electronic and atomic-scale modelling tools", *J. Phys. Condens. Matter*., **32**, 015901. https://doi.org/10.1088/1361-648X/ab4007.

Srivastava, A., Khan, M.S. (2018), "First principle study of single-electron transistor based on metal-organic complex of dibenzothiophene", *Organic Electron.*, **53**, 227-234. https://doi.org/10.1016/j.orgel.2017.11.042.

Stokbro, K. (2008), "First-principles modeling of electron transport", *J. Phys. Condens. Matter.*, **20**(6), 064216. https://doi.org/10.1088/0953-8984/20/6/064216.

Tolpygo, S.K. (2016), "Superconductor digital electronics: Scalability and energy efficiency issues", *Low Temp. Phys.*, **42**(5), 361-379. https://doi.org/10.1063/1.4948618.

Wang, P., Chen, B.B. and Wang, X. (2021), "Organic spin valves with nonvolatile memory using molecular doping", *Synthetic Met.*, **273**, 116676. https://doi.org/ 10.1016/j.synthmet.2020.116676.

Wang, Y., Zhang, S., Zhang, G., Xu, X., Zhang, C., Wang, Y. and Xie, X. (2020), "Low-drift and compact readout electronics for practical SQUID magnetocardiography working in unshielded environment", *Physica C*, **575**(7), 1353685. https://doi.org/10.1016/j.physc.2020.1353685.

Ward, D.R., Scott, G.D., Keane, Z.K., Halas, N.J. and Natelson, D. (2008), "Electronic and optical properties of electromigrated molecular junctions", *J. Phys. Condens. Matter*, **20**(37), 374118. https://doi.org/10.1088/0953-8984/20/37/374118.

Xiang, R., Inoue, T., Zheng, Y., Kumamoto, A., Qian, Y., Sato, Y., Liu, M., Tang, D., Gokhale, D., Guo, J., Hisama, K., Yotsumoto, S., Ogamoto, T., Arai, H., Kobayashi., Y., Zhang, H., Hou, B., Anisimov, A., Maruyama, M., Miyata, Y., Okada, S., Chiashi, S., Li, Y., Kong, J., Kauppinen, E.I., Ikuhara, Y., Suenaga. K. and Maruyama, S. (2020), "One-dimensional van der Waals heterostructures", *Science*, **367**(6477), 537-542. https://doi.org/10.1126/science.aaz2570.

Yang, W., Cao, Y., Han, J., Lin, X., Wang, X., Wei, G., Chen, Lv., Bournel, A. and Zhao, W. (2021), "Spin-filter induced large magnetoresistance in 2D van der Waals magnetic tunnel junctions", *Nanoscale*, **13**(2), 862-868. https://doi.org/10.1039/d0nr07290g.

Zhu, J., Chen, X., Shang, W., Ning, J., Wang, D., Zhang, J. and Hao, Y. (2021), "Van der Waals contact between 2D magnetic VSe_2 and transition metals and demonstration of high-performance spin-field-effect transistors", *Sci. China Mater*., **64**(11), 2786-2794. https://doi.org/10.1007/s40843-021-1657-9.

JL